THE JOURNAL OF BIOLOGICAL CHEMISTRY VOL. 284, NO. 9, pp. 5723–5730, February 27, 2009

Analysis of Transient and Catalytic Desosamine-binding Pockets in Cytochrome P-450 PikC from *Streptomyces venezuelae*[*]

Received for publication, October 1, 2008, and in revised form, December 10, 2008 Published, JBC Papers in Press, January 4, 2009, DOI 10.1074/jbc.M807592200

Shengying Li[‡], Hugues Ouellet[§], David H. Sherman[‡¶‖], and Larissa M. Podust[§1]

From the Life Sciences Institute, Departments of [‡]Medicinal Chemistry, [¶]Chemistry, and [‖]Microbiology & Immunology, University of Michigan, Ann Arbor, Michigan 48109 and the [§]Department of Pharmaceutical Chemistry, University of California, San Francisco, California 94158

The cytochrome P-450 PikC from *Streptomyces venezuelae* exhibits significant substrate tolerance and performs multiple hydroxylation reactions on structurally variant macrolides bearing the deoxyamino sugar desosamine. In previously determined co-crystal structures (Sherman, D. H., Li, S., Yermalitskaya, L. V., Kim, Y., Smith, J. A., Waterman, M. R., and Podust, L. M. (2006) *J. Biol. Chem.* 281, 26289–26297), the desosamine moiety of the native substrates YC-17 and narbomycin is bound in two distinct buried and surface-exposed binding pockets, mediated by specific interactions between the protonated dimethylamino group and the acidic amino acid residues Asp^{50}, Glu^{85}, and Glu^{94}. Although the Glu^{85} and Glu^{94} negative charges are essential for maximal catalytic activity of native enzyme, elimination of the surface-exposed negative charge at Asp^{50} results in significantly enhanced catalytic activity. Nevertheless, the D50N substitution could not rescue catalytic activity of $PikC_{E94Q}$ based on lack of activity in the corresponding double mutant $PikC_{D50N/E94Q}$. To address the specific role for each desosamine-binding pocket, we analyzed the x-ray structures of the $PikC_{D50N}$ mutant co-crystallized with narbomycin (1.85 Å resolution) and YC-17 (3.2 Å resolution). In $PikC_{D50N}$, the desosamine moiety of both YC-17 and narbomycin was bound in a catalytically productive "buried site." This finding suggested a two-step substrate binding mechanism, whereby desosamine is recognized in the two subsites to allow the macrolide substrate to sequentially progress toward a catalytically favorable orientation. Collectively, the binding, mutagenesis, kinetic, and x-ray structural data suggest that enhancement of the catalytic activity of $PikC_{D50N}$ is due to the facilitated relocation of substrate to the buried site, which has higher binding affinity, as opposed to dissociation in solution from the transient "surface-exposed site."

Macrolides are a large family of secondary metabolites belonging to the polyketide class of natural products generated by diverse genera of actinomycetes bacteria. The large macrolactone ring systems are derived from polymerization of simple carboxylic acid precursors catalyzed by modular polyketide synthases and often require further modification by specific tailoring enzymes (1) to acquire or enhance biological activity. The modular architecture of polyketide synthase gene clusters has led to the development of combinatorial biosynthetic approaches that aim to generate novel secondary metabolites through rational engineering of new combinations of polyketide synthase modules (2–4). Tailoring enzymes, including cytochrome P-450 monooxygenases (P-450),[2] are usually encoded within macrolide biosynthetic pathways (5). P-450 enzymes mainly serve to introduce hydroxyl or epoxide functional groups to nascent macrolactone structures or their glycosylated products (1, 3). To date, only three macrolide P-450 monooxygenases including EryF, EpoK, and PikC have been studied at both enzymatic and structural levels. Therefore, the principles of substrate recognition and regio- and stereochemical selectivity are just beginning to emerge for this intriguing group of biosynthetic enzymes.

Streptomyces venezuelae P-450 PikC displays a relatively broad substrate and regiospecificity compared with EryF (6) and EpoK (7). This characteristic combined with robust catalytic efficiency as a single component engineered biocatalyst (8) has motivated us to further its development as a prototype P-450 monooxygenase directed toward metabolic engineering and synthetic chemical applications.[3] Thus, PikC performs multiple hydroxylations of structurally variant macrolides including the 12-membered ring YC-17 and 14-membered ring narbomycin, leading to methymycin/neomethymycin and the natural ketolide antibiotic pikromycin, respectively (10) (Scheme 1). Ketolides are macrolide derivatives characterized by a C-3 keto group that have received significant attention recently because of their enhanced activity against drug-resistant microbial pathogens (11).

Both endogenous PikC substrates are glycosylated with the 3-(dimethylamino)-3,4,6-trideoxy sugar desosamine that con-

* This work was supported, in whole or in part, by National Institutes of Health Grant GM078553. This work was also supported by United States Dept. of Energy Contract DE-AC02-05CH11231. The costs of publication of this article were defrayed in part by the payment of page charges. This article must therefore be hereby marked "*advertisement*" in accordance with 18 U.S.C. Section 1734 solely to indicate this fact.

The atomic coordinates and structure factors (codes 2VZM and 2VZ7) have been deposited in the Protein Data Bank, Research Collaboratory for Structural Bioinformatics, Rutgers University, New Brunswick, NJ (http://www.rcsb.org/).

[1] To whom correspondence should be addressed: Dept. of Pharmaceutical Chemistry, University of California, 600 16th St., San Francisco, CA 54158-2280. Fax: 415-502-4728; E-mail: larissa.podust@ucsf.edu.

[2] The abbreviations used are: P-450, cytochrome P-450 monooxygenase; MOPS, 4-morpholinepropanesulfonic acid; HPLC, high pressure liquid chromatography.

[3] S. Li, M. R. Chaulagain, L. M. Podust, J. Montgomery, and D. H. Sherman, unpublished data.

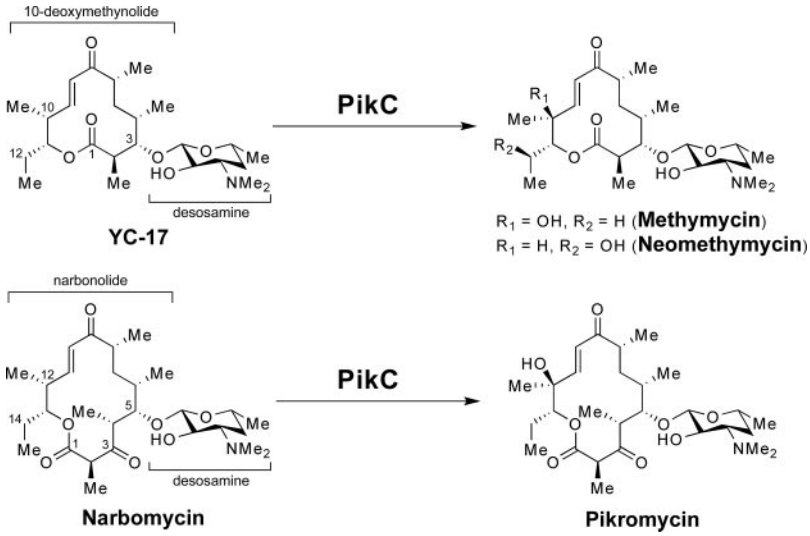

SCHEME 1. **Structures of the PikC native substrates and their hydroxylated products.**

fers antibiotic activity to a number of macrolide antibiotics such as erythromycin, troleandomycin, mycinamicin, megalomicin (desosamine), tylosin, carbomycin, spiramycin (mycaminose, having an additional hydroxyl group at the C-4 position of the sugar ring), and a highly potent semisynthetic ketolide telithromycin (11–13). PikC catalyzes hydroxylation of variant macrolide substrates modified with altered sugar moieties through metabolic engineering (14–18) or with unnatural macrolactone ring systems (19, 20). PikC has also been shown to function effectively when immobilized on a microfluidic biochip (21), and when fused to a heterologous electron donor (8), the reductase domain of a self-sufficient P-450$_{RhF}$ from *Rhodococcus* sp. NCIMB 9784 (22).

Recent analysis of the x-ray crystal structures (23) revealed that YC-17 and narbomycin bind in the PikC active site via overlapping modes sharing the macrolactone-binding site and utilizing distinct desosamine binding regions, including buried and surface-exposed pockets, respectively. In both modes, the protonated dimethylamino group of desosamine binds between two negatively charged carboxyl groups of amino acid residues forming a salt bridge with the proximal (relative to the dimethyamino moiety) carboxyl and an ionic contact with the distal one. The triad of carboxylate residues Asp^{50}, Glu^{85}, and Glu^{94} located in the BC loop provides this set of interactions. Elimination of the negative charge at Glu^{85} or Glu^{94} by site-directed mutagenesis virtually inactivates (Glu^{94}) or substantially reduces (Glu^{85}) conversion of both substrates (23). In contrast, elimination of the surface-exposed negative charge at Asp^{50} via substitution of this residue with asparagine significantly enhances catalytic activity of PikC. To address the specific role for each desosamine-binding pocket, we analyzed the x-ray structures of the catalytically superior PikC$_{D50N}$ mutant co-crystallized with narbomycin or YC-17. In PikC$_{D50N}$, YC-17 adopts the same binding mode as observed previously in the wild type, with desosamine bound in the buried pocket. In contrast to the previously observed binding mode in wild type PikC, narbomycin was also found predominantly in the buried pocket in the corresponding D50N mutant form, suggesting the possibility of initial substrate recognition in the "surface-exposed site," with subsequent relocation to the catalytic "buried site." We herein report PikC substrate binding, enzyme mutagenesis, and kinetic data to support this hypothesis and provide evidence for kinetic control over substrate dissociation *versus* relocation to the PikC catalytic pocket.

EXPERIMENTAL PROCEDURES

Preparation of Protein Samples—Expression vectors for PikC wild type and mutants were used to transform *Escherichia coli* strain HMS174(DE3) to express and subsequently purify proteins according to the protocol described elsewhere (23). The double mutants PikC$_{D50N/E94Q}$ and PikC$_{D50N/E85Q}$ represent new constructs prepared in this study. The quality of the purified proteins was assessed by the SDS-PAGE and UV-visible spectroscopy, and the concentration was determined at 450 nm from the difference spectra between the carbon monoxide-bound ferrous and water-bound ferric forms using the extinction coefficient of 91,000 M^{-1} cm^{-1} (24).

Preparation of Substrates—Substrates YC-17 and narbomycin were obtained from the *pikC* knock-out strain *S. venezuelae* AX-906 (10). Alternatively, narbomycin was harvested from fermentation culture of *Streptomyces narbonensis* NRRL B-1680 in soluble complete medium, containing 15 g of soluble starch, 20 g of soytone, 1.5 g of yeast extract, 10.5 g of MOPS, 0.1 g of $CaCl_2$ at pH 7.2, per 1 liter of deionized water.

Equilibrium Binding Assay—Spectroscopic substrate binding assay was carried out at room temperature using a UV-visible spectrophotometer 300 Bio (Cary). Protein dissolved in 50 mM sodium phosphate, pH 7.3, 1 mM EDTA, 0.2 mM dithioerythritol, and 10% glycerol at concentrations ranging from 1 to 2 μM was titrated with the substrate dissolved in Me_2SO (20 mM) in 1-μl aliquots. The same amounts of Me_2SO alone were added to the protein in the reference cuvette followed by recording of the difference spectra. Absorbance differences ΔA ($A_{peak\ 389\ nm} - A_{trough\ 422\ nm}$) were plotted *versus* substrate concentration, and data from duplicated experiments were fitted to the hyperbolic function $\Delta A = (A_{max}(S/K_D + S)$, where S is the total ligand concentration, A_{max} is the maximal absorption shift at saturation, and K_D is the apparent dissociation constant for the enzyme-ligand complex.

Catalytic Activity Assay—Enzymatic conversion of YC-17 or narbomycin *in vitro* were performed using a previously developed assay (10). The standard reaction contained 1 μM PikC (wild type or mutant form), 0.5 mM YC-17 or narbomycin, 3.5 μM spinach ferredoxin, 0.01 units of spinach ferredoxin-$NADP^+$ reductase, and 1 mM NADPH in 100 μl of 50 mM sodium phosphate, pH 7.3, 1 mM EDTA, 0.2 mM dithioerythritol, and 10% (v/v) glycerol. The reaction was terminated after 40 min of incubation at 30 °C by the addition of 3 × 300 μl of chloroform. The extractions were subsequently combined,

TABLE 1
Data collection and refinement statistics

Parameter	Value(s)[a] or determination	
	Narbomycin (Protein Data Bank code 2VZM)	YC-17 (Protein Data Bank code 2VZ7)
Wavelength (Å)	1.11587	1.11587
Resolution (Å)	1.85	3.2
Unique reflections	87273	17248
Redundancy	3.9 (3.1)	4.3 (4.4)
Completeness (%)	98.7 (90.0)	100.0 (99.9)
Space group	$P2_12_12_1$	$P2_12_12_1$
Cell dimensions: *a*, *b*, *c* (Å)	60.4, 109.5, 153.1	59.9, 109.3, 153.0
Molecules in asymmetric unit	2	2
Solvent content (%)	53	53
R_{sym} (%)[b]	6.5 (33.1)	12.8 (46.3)
I/σ	23.8 (2.3)	9.9 (2.7)
Refinement		
Reflections used in refinement	77423	16262
R_{crys}/R_{free} (%)[c]	16.5/21.1	17.9/26.0
No. of atoms		
Protein	6233	6116
Prosthetic groups and ligands	158	150
Water	641	176
Wilson plot *B* values (Å^2)	22.4	50.6
Mean *B* factor (Å^2)	24.4	46.7
Protein	23.7	45.1
Heme	12.9	28.9
Substrate	32.7	41.7
Water	31.4	29.6
Root mean square deviation deviations		
Bond length (Å)	0.016	0.008
Bond angles (°)	1.6	1.3
Ramachandran statistics (%)[d]		
A	93.5/5.6/0.3/0.6	84.0/14.8/1.2/0.0
B	92.0/8.0/0.0/0.0	84.8/14.9/0.3/0.0

[a] The numbers in parentheses correspond to the highest resolution shell.
[b] $R_{sym} = \Sigma|I_i - <I>|/\Sigma I_i$, where I_i is the intensity of the i^{th} observation and $<I>$ is the mean intensity of reflection.
[c] $R_{cryst} = \Sigma||F_o| - |F_c||/\Sigma|F_o|$, calculated with the working reflection set. R_{free} is the same as R_{cryst} but calculated with the reserved reflection set.
[d] Program PROCHECK, portions of the protein residues in most favored/additional allowed/generously allowed/disallowed regions.

dried, and dissolved in 120 μl of methanol and subjected to the reverse phase HPLC using a X-Bridge C18, 5 μm, 250-mm column (Waters Corporation) in a linear gradient (30–60%) of acetonitrile in 10 mM ammonium acetate, pH 8.1, at the flow rate of 1.0 ml/min. Detection was at 238 nm.

Pre-steady State Binding Assay—Stopped flow kinetic analysis experiments were conducted at 23 °C using a Hi-Tech Scientific instrument equipped with a photodiode array detector and controlled by the KinetAsyst software (Bradford on Avon, UK). Protein and narbomycin solutions were prepared in 50 mM Tris-HCl, pH 7.5, and 0.5 mM EDTA. Narbomycin stock solution was in Me_2SO; therefore, solvent concentration was adjusted in both syringes and maintained constant (0.5%) throughout the experiments. Protein concentration after mixing was 10 μM. To maintain pseudo first order reaction conditions, all of the measurements were carried out in 10-fold excess of narbomycin over the protein. Kinetic transients were recorded for 0.5 s at 390 nm corresponding to the peak of the difference spectra between the high spin substrate-bound and the low spin substrate-free PikC forms. Multiple kinetic traces for each sample were measured and averaged prior to data analysis. The data points from 2 to 500 ms were fitted to a standard double exponential function using SPECFIT software.

Crystallization and Data Collection—$PikC_{D50N}$ from the 1 mM frozen stock stored at −80 °C in 20 mM Tris-HCl, pH 7.5, 200 mM NaCl, and 0.5 mM EDTA was mixed with either YC-17 or narbomycin, both dissolved in Me_2SO at 50 mM stock concentration, to final concentrations of 0.2 mM for protein and 2 mM for the ligand. The mixtures were subjected to the automated screening of crystallization conditions (hanging drop crystallization protocol) using a nanoliter drop setter Mosquito (TTP LabTech) and commercial high throughput screening kits purchased from Hampton Research and Qiagen. Crystallization conditions generating crystals were identified and optimized further in 24-well crystallization plates. The crystals used for x-ray data collection were obtained at 23 °C for the $PikC_{D50N}$-YC-17 complex from 20% polyethylene glycol 4000, 0.1 M Bis-Tris, pH 6.5, and 0.2 M Li_2SO_4, and for the $PikC_{D50N}$-narbomycin complex from 16% polyethylene glycol 8000, 0.1 M sodium cacodilate, pH 6.5, and 0.15 M Li_2SO_4. Prior to data collection, the crystals were cryo-protected by plunging into a drop of reservoir solution supplemented with 20% glycerol and flash frozen in the liquid nitrogen. Diffraction data were collected at 100–110 K at beamline 8.3.1, Advanced Light Source, Lawrence Berkeley National Laboratory. The images were integrated, and the intensities were merged by using the HKL2000 software suite (25).

Structure Determination and Refinement—Structures were determined by molecular replacement using the CCP4 (26) program suit and an A chain of the YC-17-bound PikC (Protein Data Bank code 2C6H) as a search model. Model building was performed with the programs COOT (27, 28) and O (29) and refined using REFMAC5 (26, 30). Simulated annealing was performed, and electron density composite omit maps were generated using CNS (31). The data collection and refinement statistics are shown in Table 1.

RESULTS

Substrate Binding—Binding affinities of PikC wild type and the mutants for the native substrates, YC-17 and narbomycin, and their aglycone precursors, 10-deoxymethynolide and narbonolide, were deduced from a low to high spin iron spectral shift, known as type I binding (32). Both narbonolide and 10-deoxymethynolide bound PikC with the significantly reduced affinities compared with the corresponding glycosylated substrates (Table 2), which may explain, at least in part, lack of hydroxylation by PikC. Binding affinity for YC-17 (K_D = 98.9 μM) was 2.3 times higher than narbomycin (234.5 μM) (Fig. 1, *panels A1 and B1*). Compared with wild type enzyme, binding affinities of the catalytically more active $PikC_{D50N}$ increased about 4-fold for YC-17 (27.2 μM) and 1.3-fold for narbomycin (171.9 μM) (*panels A2/B2*). $PikC_{E85Q}$ had reduced binding affinities for both substrates compared with wild type enzyme (*panels A3/B3*). Binding affinities for $PikC_{E94Q}$ were even further reduced (*panels A4/B4*), although the K_D values could not be determined for YC-17 because saturation of enzyme could not be approached because of both low binding affinity and limited substrate solubility. Additionally, D50N substitution did not significantly affect binding in the double mutants (Table 2 and Fig. 1, *panels 5* and *6*).

TABLE 2

The values of dissociation constants (K_D) for natural PikC substrates and their aglycones

Enzyme	K_D		K_D	
	YC-17	Narbomycin	10-Deoxymethynolide	Narbononolide
	μM		mM	
$PikC_{wild\ type}$	98.9 ± 1.9	234.5 ± 15.0	2.1 ± 0.8	21.1 ± 12.2
$PikC_{D50N}$	27.2 ± 0.6	171.9 ± 14.7	0.9 ± 0.3	2.1 ± 1.5
$PikC_{E85Q}$	340.3 ± 31.5	351.6 ± 54.1	ND[b]	ND
$PikC_{E94Q}$	–[a]	1056.8 ± 212.4	ND	ND
$PikC_{D50N/E85Q}$	289.6 ± 28.8	459.0 ± 64.7	ND	ND
$PikC_{D50N/E94Q}$	–[a]	861.0 ± 567.4	ND	ND

[a] Binding curves (Fig. 1, *panels A4* and *A6*) could not be fitted.
[b] ND, not determined.

Kinetics of Narbomycin Binding—Binding of narbomycin to PikC wild type and the $PikC_{D50N}$ and $PikC_{E85Q}$ mutants was addressed by stopped flow UV-visible spectroscopy. Binding kinetics were biphasic and accurately described by a double exponential function revealing a fast first phase followed by a slow second one (Fig. 2). The kinetic rate of the first binding step (accounting for ~50% of the reaction amplitude) was fast and protein-dependent (Table 3). The rate of the second step was slow, 13 s^{-1}, and virtually identical between the wild type and both mutant forms (D50N and E85Q) of PikC. The first binding rate of the catalytically superior $PikC_{D50N}$ was twice as fast as that of the low activity mutant $PikC_{E85Q}$: 822.8 ± 21.8 s^{-1} *versus* 421.4 ± 18.4 s^{-1}, respectively, with the wild type determined to be more similar to the D50N mutant at 703.0 ± 29.1 s^{-1}. We assume that the first binding step represents a pseudo first order reaction of the bimolecular encounter between PikC and narbomycin, whereas the second slow step may reflect monomolecular conformational adjustments of

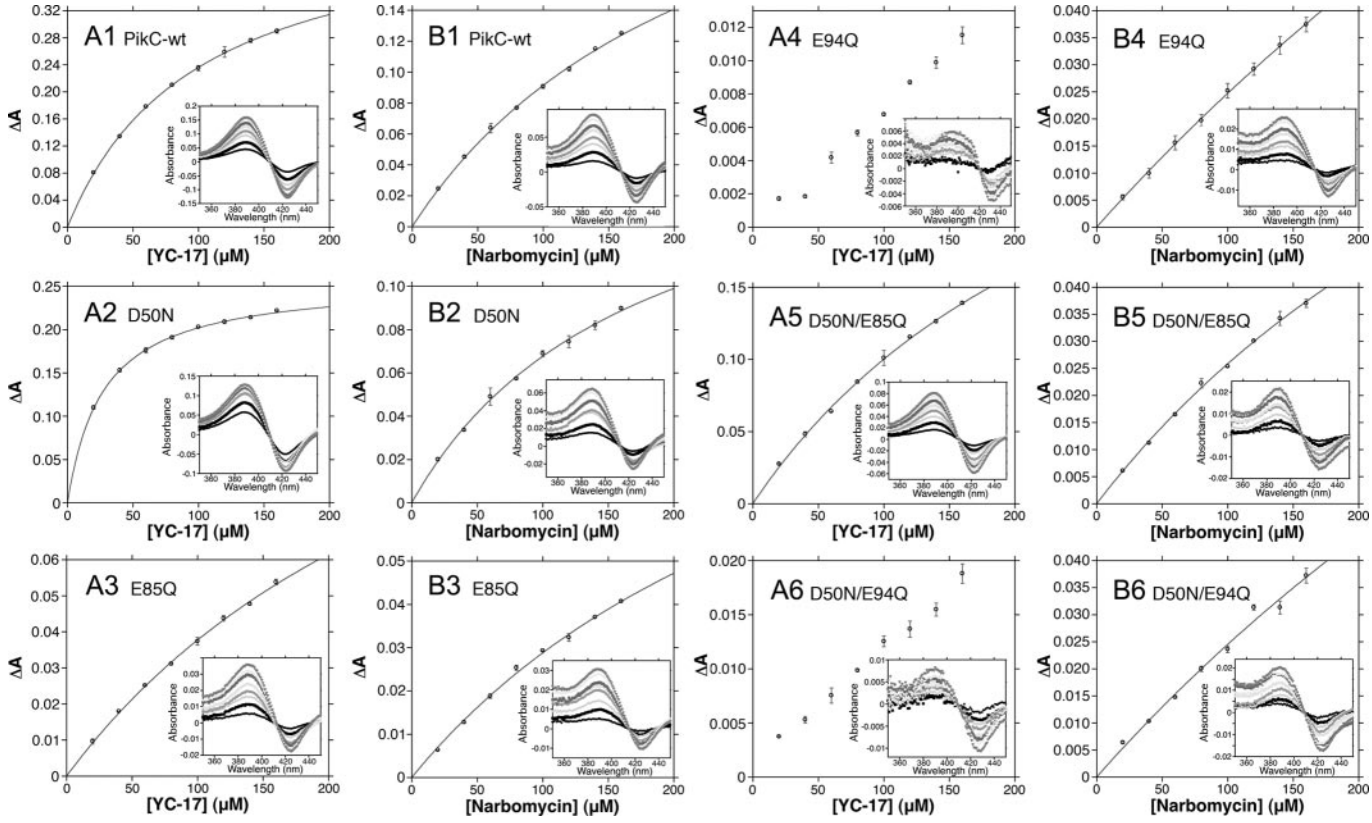

FIGURE 1. **Binding of YC-17 and narbomycin to PikC.** The concentration dependence of YC-17 (*A panels*) and narbomycin (*B panels*) binding deduced from the difference absorption changes (shown in *insets*) obtained from titration of PikC wild type or mutant enzymes, as indicated in each panel with increasing concentrations of substrates, as shown. Titration experiments were performed in 50 mM sodium phosphate, pH 7.3, 1 mM EDTA, 0.2 mM dithioerythritol, and 10% glycerol. The absence of the fitting curves in *panels A4* and *A6* indicates an unsuccessful fit caused by a lack of enzyme saturation. The values for the binding constants obtained from the curve fitting are presented in Table 2.

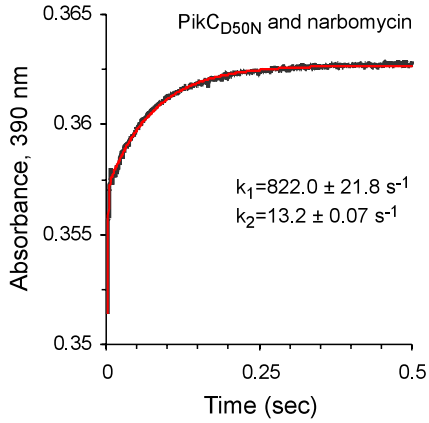

FIGURE 2. **Kinetics of narbomycin binding.** Typical kinetic transient of narbomycin binding (*black*) fitted to a double exponential function (*red*) is shown for PikC$_{D50N}$. Stopped flow experiments were conducted in 50 mM Tris-HCl, pH 7.5, 0.5% Me_2SO, and 0.5 mM EDTA.

TABLE 3

Pre-steady state kinetic parameters of narbomycin binding

Enzyme	k_1	k_2
	s^{-1}	s^{-1}
PikC$_{wild\ type}$	703.0 ± 29.1	13.5 ± 0.08
PikC$_{D50N}$	822.0 ± 21.8	13.2 ± 0.07
PikC$_{E85Q}$	421.4 ± 18.4	13.7 ± 0.10

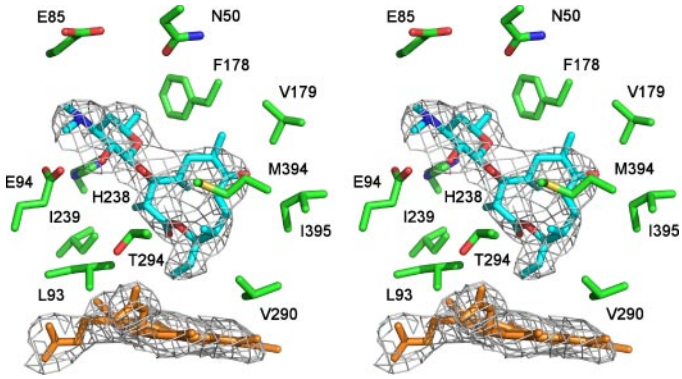

FIGURE 3. **YC-17 binding in PikC$_{D50N}$.** Stereo view of YC-17 (highlighted in *cyan*) bound in the active site of PikC$_{D50N}$ (Protein Data Bank code 2VZ7, chain A) surrounded by heme and amino acid side chains (*green*) within 4 Å plus N50 is shown. Fragments of the $2F_o - F_c$ electron density composite omit map contoured at 0.8 σ are shown as *gray mesh*. Heme is *orange*, nitrogen atoms are *blue*, and oxygen atoms are *red*. The image was generated using PYMOL program (38).

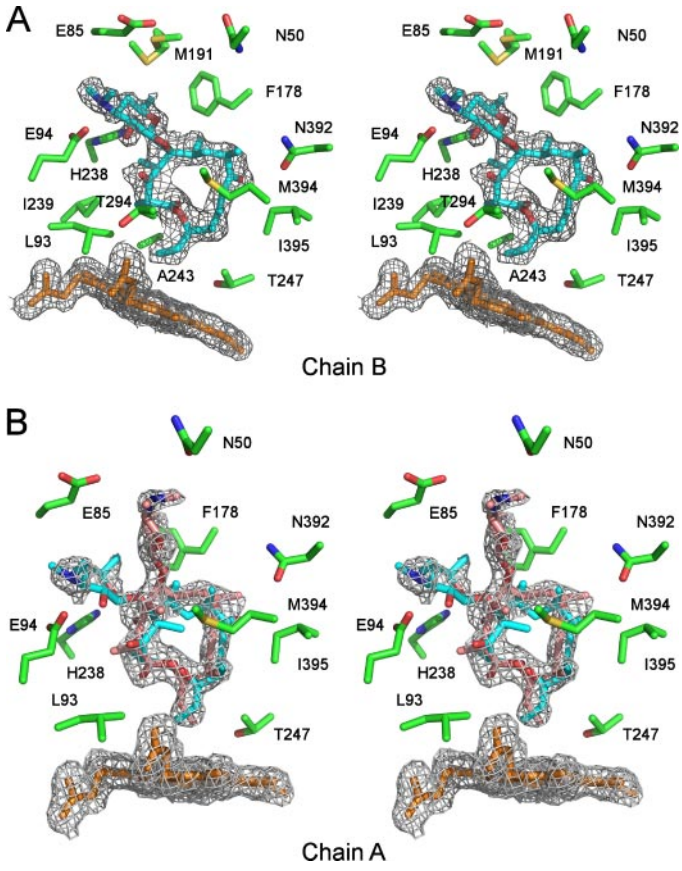

FIGURE 4. **Narbomycin binding in PikC$_{D50N}$.** Stereo views of narbomycin (*cyan or pink*) bound in the active site of PikC$_{D50N}$ (Protein Data Bank code 2VZM) (*A*) in the chain B and (*B*) in the chain A are shown. Selected amino acid side chains (*green*) are within 4 Å. In *A*, alternative conformations for Met^{191} are shown. Heme is in *orange*, nitrogen atoms are in *blue*, oxygen atoms are in *red*, and sulfur atoms in *yellow*. Fragments of the $2F_o - F_c$ electron density composite omit map contoured at 0.8 σ are shown as *gray mesh*.

substrate position in the active site assisted by PikC dynamics (23). Because of small changes in the absolute spectra used to monitor the reaction and the limited solubility of narbomycin, we were unable to accurately estimate the k_{on} from the concentration dependence of the observed rates. Also, the pseudo first order rate for PikC$_{D50N}$ may be underestimated because of instrument limitations for monitoring fast reactions.

X-ray Structure of the PikC$_{D50N}$-YC-17 Complex—The crystal structure of the PikC$_{D50N}$-YC-17 complex was determined to a resolution of 3.2 Å (Table 1). Although determined at relatively low resolution, the electron density for YC-17 in both protein monomers in an asymmetric unit was well defined, showing no ambiguity for macrolide binding (Fig. 3). In both monomers (superimposable with the root mean square deviation of 0.43 Å), YC-17 was bound in the active site with desosamine positioned in the buried pocket anchored via the dimethylamino group to the side chain of Glu^{94} and Glu^{85}, similar to what has been observed for wild type PikC (23).

X-ray Structure of the PikC$_{D50N}$-Narbomycin Complex—Although they share the same space group and the unit cell dimensions as the PikC$_{D50N}$-YC-17 (Table 1), PikC$_{D50N}$-narbomycin crystals diffracted to a higher resolution (1.85 Å), revealing new details of the protein-substrate interactions. Although two protein monomers in the asymmetric unit had virtually identical overall conformations (root mean square deviation of 0.34 Å), the desosamine moiety of narbomycin was found in both alternative pockets. In the chain B form, desosamine was unambiguously bound in the buried pocket with the dimethylamino group positioned between the Glu^{94} and Glu^{85} side chains (Fig. 4*A*). This binding mode has been previously characterized for YC-17 but not for narbomycin (23). In the chain A form, electron density for the macrolactone ring of narbomycin was clearly defined, whereas electron density for desosamine was split between both buried and surface-exposed pockets, suggesting two alternative conformations (Fig. 4*B*), each refined with the occupancy of 0.5. The buried conformation (*cyan* in Fig. 4*B*) superimposed well between the A and B monomer, whereas the surface-exposed conformation in monomer A (*pink*) superimposed with the position observed for narbo-

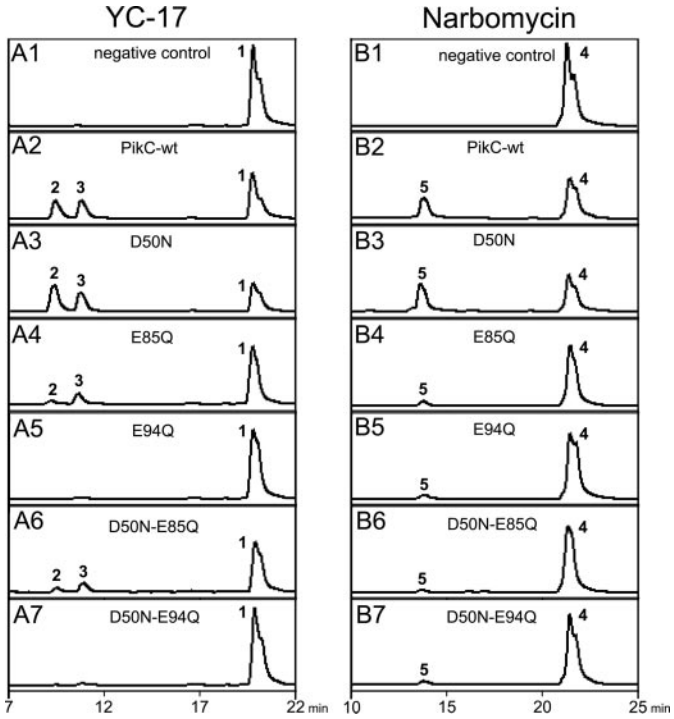

FIGURE 5. **Catalytic activity of PikC mutants.** High pressure liquid chromatography analysis of PikC-catalyzed reactions using YC-17 (*A panels*) and narbomycin (*B panels*) as substrate are shown. *A1/B1*, negative control in the absence of PikC. *A2/B2*, PikC wild type (PikC-wt). The mutants are used as indicated in the figure. The compound identities are as follows: **1**, YC-17; **2**, neomethymycin; **3**, methymycin; **4**, narbomycin; **5**, pikromycin. The peak identity in each HPLC trace was determined by mass spectrometry and compared with authentic compounds with respect to HPLC retention time and UV spectrum. The area under each peak was quantified, and the results for each chromatogram are presented in Table 4.

TABLE 4

Conversion of YC-17 and narbomycin by different PikC forms represented in Fig. 5

Enzyme	Panel in Fig. 5	Conversion of YC-17		Conversion of narbomycin (% of total)
		% of total	Product 2:3 ratio	
PikC-wt	*A2/B2*	40.0	0.81	35.0
D50N	*A3/B3*	60.0	1.15	44.4
E85Q	*A4/B4*	18.0	0.26	8.1
E94Q	*A5/B5*	0		5.4
D50N/E85Q	*A6/B6*	18.4	0.38	3.5
D50N/E94Q	*A7/B7*	0		5.3

mycin in the wild type enzyme (23). Interestingly, in the surface-exposed pocket of $PikC_{D50N}$, the dimethylamino group of desosamine was located between the carboxyl group of Glu^{85} and the carboxamide group of Asn^{50} substituting for Asp^{50}. In addition, subtle differences were observed for the macrolactone portion of narbomycin between the two binding modes (Fig. 4*B*).

Catalytic Activity of PikC Mutants—The catalytic activity of the double mutants $PikC_{D50N/E94Q}$ and $PikC_{D50N/E85Q}$ was addressed simultaneously with the panel of single PikC mutants characterized previously (23). Enhanced catalytic activity for $PikC_{D50N}$ and attenuated catalytic activity for $PikC_{E94Q}$ were confirmed (Fig. 5 and Table 4). As before, residual catalytic conversion by $PikC_{E94Q}$ was observed for narbomycin, 5.4% *versus* 35.0% for the wild type, but not for YC-17 (Fig. 5, *panels A5* and *B5* and Table 4). In accord with previous results (23), E85Q substitution notably reduced but did not entirely eliminate both catalytic activities (Fig. 5, *panels A4/B4*, and Table 4). Significantly, introduction of the D50N substitution failed to rescue catalytic activity of the double mutants (Fig. 5, compare *panels 4* and *5* with *panels 6* and *7*, respectively), revealing the dominant impact of the E94 interaction for PikC function.

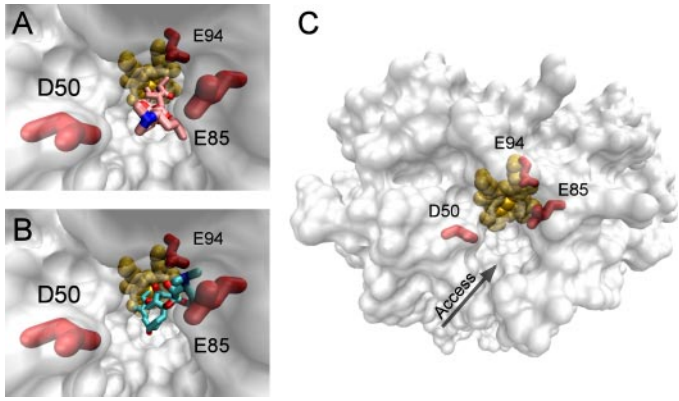

FIGURE 6. **Transient and catalytic desosamine-binding pockets.** (*A*) Narbomycin in the surface-exposed pocket is highlighted in *pink*. (*B*) Narbomycin in the buried pocket is highlighted in *cyan*. Zoomed images in (*A*) and (*B*) are shown in perspective. (*C*) Semi-transparent surface of the $PikC_{D50N}$ shows overall disposition of the negatively charged residues. Heme (*orange*) is shown as van der Waals' spheres. N atoms of desosamine are *blue*, O atoms *red*. Carboxylic residues Asp^{50}, Glu^{85}, and Glu^{94} are shown as *red sticks*. Images were generated using VMD program (9).

DISCUSSION

Desosamine plays a fascinating parallel role both in targeting macrolide molecules to the 50 S bacterial ribosomal subunit (33, 34) and in tailoring of these important antibiotics by biosynthetic P-450 enzymes. In each case, the *N,N*-dimethylamino group of the sugar provides a key interaction for anchoring the macrolactone in its specific binding site. Antibiotic action is achieved through blockage of the peptide exit site resulting from precise macrolide interactions (35). Sugar anchoring also provides the basis for hydroxylation in the active site of P-450 monooxygenases PikC (23), EryK (36), MycCI, and MycG (37). As shown previously for PikC, the specific interactions between the protonated dimethylamino group of desosamine and the carboxyl-containing residues in the binding site are required for the catalytic activity. Nonglycosylated substrate precursors narbonolide and 10-deoxymethynolide, are very weakly bound with K_D values in the millimolar range (Table 2) and do not serve as substrates for PikC. Thus, given the importance of negative charges associated with Glu^{85} and Glu^{94}, the enhancement of catalytic activity in $PikC_{D50N}$ was surprising.

In a search for determinants of improved catalytic function of $PikC_{D50N}$, we have determined the x-ray structures for this mutant complexed with the native substrates YC-17 and narbomycin. Although YC-17 showed no binding ambiguity (Fig. 3), narbomycin adopted two alternative conformations in the active site of the mutant enzyme (Figs. 4 and 6). Moreover, for the 14-membered ring macrolide, 25% of protein molecules in the $PikC_{D50N}$-narbomycin crystals had desosamine bound in the surface-exposed pocket, whereas the remaining molecules revealed desosamine associated with the buried pocket. The

latter binding mode has not been observed for narbomycin previously. In the surface-exposed pocket of $PikC_{D50N}$, the dimethylamino group of desosamine formed a salt bridge to the proximal Glu^{85} residue as it does in the wild type. However, the original ionic contact with the distal Asp^{50} was no longer available because of removal of the negative charge through asparagine substitution. We surmised that the loss of an electrostatic component might weaken protein-desosamine interactions in the surface-exposed pocket and facilitate desosamine relocation to the buried position, suggesting a catalytic role for this site. If so, the $PikC_{D50N/E94Q}$ double mutant should remain sensitive to the E94Q substitution. Alternatively, if D50N substitution favors hydroxylation from the surface-exposed pocket (given that the macrolactone is positioned similarly in respect to the iron center in both binding modes (Fig. 4*B*)), $PikC_{D50N/E94Q}$ should be insensitive to the E94Q mutation. To test both hypotheses, the catalytic activities of two double mutants, $PikC_{D50N/E94Q}$ and $PikC_{D50N/E85Q}$, were analyzed. The D50N substitution could not rescue or even affect the functional activity of the double mutants (Fig. 5 and Table 4), supporting the facilitated relocation to the buried pocket as a factor that favors catalysis.

Both the PikC mutagenesis studies and the crystal structure analysis suggest a two-step substrate binding mechanism whereby desosamine of the macrolide substrate initially binds to the surface-exposed pocket (Fig. 6*A*) and then relocates to the catalytic buried site (Fig. 6*B*). Because narbomycin is comprised of a 14-membered macrolactone ring, it could have a higher energetic barrier for conversion from one site to another and therefore was trapped entirely in the surface-exposed pocket in the crystals of the wild type enzyme (23) and partially in the crystals of the $PikC_{D50N}$ mutant. The hampered relocation to the buried pocket might explain the reduced binding affinity of narbomycin compared with YC-17: 234.5 ± 15.0 μM *versus* 98.9 ± 1.9 μM (Table 2), because the substrate is presumed to be more easily released from the surface-exposed pocket than the buried one. Accordingly, the affinity of $PikC_{D50N}$ is higher toward both substrates because of facilitated access for desosamine to the buried pocket, which reduces dissociation of substrate from the surface-exposed site. Thus, the residual level of the $PikC_{E94Q}$ catalytic activity toward narbomycin (Fig. 5, *panel B5*, and Table 4) is readily explained by marginal hydroxylation from the surface-exposed pocket. In contrast, YC-17 is not hydroxylated by this mutant (Fig. 5, *panel A5*) because of rapid relocation to the buried pocket, where catalytic activity depends entirely on the interactions with Glu^{94}.

The residual level of hydroxylation demonstrated by $PikC_{E85Q}$ toward both substrates (Fig. 5, *panels A4* and *B4*, and Table 4) suggests that relocation of each macrolide is affected in this mutant. Glu^{85} is centered between the two pockets (Fig. 6) and therefore may serve as a pivot in the transition of desosamine, because the latter may remain electrostatically "tethered" to the Glu^{85} carboxylate group during the relocation. Because introduction of the D50N substitution could not rescue catalysis (Fig. 5, *panels A6* and *B6*, and Table 4), the residual hydroxylation by $PikC_{E85Q}$ is likely to occur from the surface-exposed pocket as well.

Because of the dynamic constraints imposed upon narbomycin, we were able to assess kinetic binding rates between the PikC mutants by UV-visible spectroscopy combined with stopped flow kinetic studies. The kinetic trends were consistent with the equilibrium binding and functional data, because the catalytically superior $PikC_{D50N}$ bound narbomycin twice as fast as the poorly active $PikC_{E85Q}$ mutant enzyme under the same experimental conditions (Table 3). This observation suggests that the first kinetic rate likely reflects formation of the final buried complex rather than a transient one, and hence, transition from the surface-exposed to the buried site is the rate-limiting step of the substrate binding reaction.

The regiospecificity of PikC is a particularly interesting characteristic of this enzyme. In all PikC/substrate co-crystal structures reported to date, the allylic carbon hydroxylation center in YC-17 (C-10) and narbomycin (C-12) is >7 Å away from the iron. The allylic C-H bond is the predominant hydroxylation site in narbomycin and one of two equally hydroxylated sites in YC-17, the second (methylene at C-12) positioned within 5 Å from the iron. Differences in the ratio of the YC-17 hydroxylation products between $PikC_{D50N}$, $PikC_{E85Q}$, and the wild type (Fig. 5 and Table 4) may be explained by dynamic variations in substrate binding making one site more favorably positioned for hydroxylation. At the same time, despite its 5 Å proximity to the iron reaction center, we have not observed hydroxylation of the methylene C-14 site in narbomycin by any PikC form *in vitro*, suggesting the possibility of additional steric or electronic factors that shift hydroxylation to the allylic C-12 site exclusively.

Collectively, our data indicate that each of the triad carboxylic acid residues interacting with the positive charge of desosamine plays a particular role in PikC catalysis; surface-exposed Asp^{50} appears to function as a gate for substrate access to the active site through kinetic control over substrate dissociation in solution from the transient site *versus* transition to the catalytic buried site. Glu^{85} centered between two desosamine-binding pockets may serve as a pivot in desosamine relocation. Finally, Glu^{94} evidently plays a major role in tuning substrate orientation for effective catalysis.

Acknowledgments—We thank Dr. Paul Ortiz de Montellano for valuable contributions, Dr. Chris Waddling for the assistance with the software and instrumentation in the UCSF X-ray Facility, and personnel of the Advanced Light Source beamline 8.3.1, Lawrence Berkeley National Laboratory: James Holton, George Meigs and Jane Tanamachi, for assistance with data collection.

REFERENCES

1. Rix, U., Fischer, C., Remsing, L. L., and Rohr, J. (2002) *Nat. Prod. Rep.* **19,** 542–580
2. Hutchinson, C. R. (1998) *Curr. Opin. Microbiol.* **1,** 319–329
3. Walsh, C. T. (2002) *Chembiochem.* **3,** 125–134
4. Sherman, D. H. (2005) *Nat. Biotechnol.* **23,** 1083–1084
5. Podust, L. M., Bach, H., Kim, Y., Lamb, D. C., Arase, M., Sherman, D. H., Kelly, S. L., and Waterman, M. R. (2004) *Protein Sci.* **13,** 255–268
6. Andersen, J. F., Tatsuta, K., Gunji, H., Ishiyama, T., and Hutchinson, C. R. (1993) *Biochemistry* **32,** 1905–1913
7. Ogura, H., Nishida, C. R., Hoch, U. R., Perera, R., Dawson, J. H., and Ortiz de Montellano, P. R. (2004) *Biochemistry* **43,** 14712–14721

8. Li, S., Podust, L. M., and Sherman, D. H. (2007) *J. Am. Chem. Soc.* **129,** 12940–12941
9. Humphrey, W., Dalke, A., and Schulten, K. (1996) *J. Mol. Graph.* **14,** 33–38
10. Xue, Y., Wilson, D., Zhao, L., Liu, H.-w., and Sherman, D. H. (1998) *Chem. Biol.* **5,** 661–667
11. Ma, Z., and Nemoto, P. A. (2002) *Curr. Med. Chem.* **1,** 15–34
12. Ackermann, G., and Rodloff, A. C. (2003) *J. Antimicrob. Chemother.* **51,** 497–511
13. Blasi, F., Cazzola, M., Tarsia, P., Aliberti, S., Baldessari, C., and Valenti, V. (2006) *Future Microbiol.* **1,** 7–16
14. Zhao, L., Sherman, D. H., and Liu, H.-W. (1998) *J. Amer. Chem. Soc.* **120,** 10256–10257
15. Zhao, L., Que, N. L. S., Xue, Y., Sherman, D. H., and Liu, H.-W. (1998) *J. Am. Chem. Soc.* **120,** 12159–12160
16. Zhao, L., Ahlert, J., Xue, Y., Thorson, J. S., Sherman, D. H., and Liu, H.-W. (1999) *J. Amer. Chem. Soc.* **121,** 9881–9882
17. Borisova, S. A., Zhao, L., Sherman, D. H., and Liu, H. W. (1999) *Org. Lett.* **1,** 133–136
18. Tang, L., and McDaniel, R. (2001) *Chem. Biol.* **8,** 547–555
19. Khosla, C., Gokhale, R. S., Jacobsen, J. R., and Cane, D. E. (1999) *Annu. Rev. Biochem.* **68,** 219–253
20. Yoon, Y. J., Beck, B. J., Kim, B. S., Kang, H. Y., Reynolds, K. A., and Sherman, D. H. (2002) *Chem. Biol.* **9,** 203–214
21. Srinivasan, A., Bach, H., Sherman, D. H., and Dordick, J. S. (2004) *Biotechnol. Bioeng.* **88,** 528–535
22. Nodate, M., Kubota, M., and Misawa, N. (2006) *Appl. Microbiol. Biotechnol.* **71,** 455–462
23. Sherman, D. H., Li, S., Yermalitskaya, L. V., Kim, Y., Smith, J. A., Waterman, M. R., and Podust, L. M. (2006) *J. Biol. Chem.* **281,** 26289–26297
24. Omura, T., and Sato, R. (1964) *J. Biol. Chem.* **239,** 2379–2385
25. Otwinowski, Z., and Minor, W. (1997) *Methods Enzymol.* **276,** 307–326
26. (1994) *Acta Crystallogr. Sect. D Biol. Crystallogr.* **50,** 760–763
27. Vagin, A., and Teplyakov, A. (1997) *J. Appl. Crystallogr.* **30,** 1022–1025
28. Emsley, P., and Cowtan, K. (2004) *Acta Crystallogr. D Biol. Crystallogr.* **60,** 2126–2132
29. Jones, T. A., Zou, J. Y., Cowan, S. W., and Kjeldgaard, M. (1991) *Acta Crystallogr. Sect. A* **47,** 110–119
30. Murshudov, G. N., Vagin, A. A., and Dodson, E. J. (1997) *Acta Crystallogr. D Biol. Crystallogr.* **53,** 240–255
31. Brunger, A. T., Adams, P. D., Clore, G. M., Delano, W. L., Gros, P., Grosse-Kunstleve, R. W., Jiang, J.-S., Kuszewski, J., Nilges, M., and Pannu, N. S. (1998) *Acta Crystallogr. Sect. D Biol. Crystallogr.* **54,** 905–921
32. Schenkman, J. B., Remmer, H., and Estabrook, R. W. (1967) *Mol. Pharmacol.* **3,** 113–123
33. Hansen, J. L., Ippolito, J. A., Ban, N., Nissen, P., Moore, P. B., and Steitz, T. A. (2002) *Mol. Cell* **10,** 117–128
34. Auerbach, T., Bashan, A., and Yonath, A. (2004) *Trends Biotechnol.* **22,** 570–576
35. Jenni, S., and Ban, N. (2003) *Curr. Opin. Struct. Biol.* **13,** 212–219
36. Lambalot, R. H., Cane, D. E., Aparicio, J. J., and Katz, L. (1995) *Biochemistry* **34,** 1858–1866
37. Anzai, Y., Li, S., Chaulagain, M. R., Kinoshita, K., Kato, F., Montgomery, J., and Sherman, D. H. (2008) *Chem. Biol.* **15,** 950–959
38. DeLano, W. L. (2002) *The PyMOL Molecular Graphics System*, DeLano Scientific, San Carlos, CA

Analysis of Transient and Catalytic Desosamine-binding Pockets in Cytochrome P-450 PikC from *Streptomyces venezuelae*

Shengying Li, Hugues Ouellet, David H. Sherman and Larissa M. Podust

J. Biol. Chem. 2009, 284:5723-5730.
doi: 10.1074/jbc.M807592200 originally published online January 4, 2009
